Acta Cryst. (1998). B**54**, 774–781

Multipole Analysis of the Electron Density in Topaz Using X-ray Diffraction Data

Yu. V. Ivanov,[a] E. L. Belokoneva,[b] J. Protas,[c]* N. K. Hansen[c] and V. G. Tsirelson[a]

[a]*Department of Physics, Mendeleev University of Chemical Technology, Miusskaya Sq. 9, Moscow 125047, Russia,* [b]*Department of Crystallography and Crystal Chemistry, Moscow State University, Leninskiye Gory, Moscow 119899, Russia, and* [c]*Laboratoire de Cristallographie et Modélisation des Matériaux Minéraux et Biologiques, URA-CNRS 809, Université Henri Poincaré-Nancy 1, BP239, F-54506 Vandoeuvre lès Nancy CEDEX, France.*
E-mail: protas@lcm3b.u-nancy.fr

(*Received 2 June 1997; accepted 19 March 1998*)

Abstract

The static deformation electron density, Laplacian of the electron density and critical points in the electron density were analyzed in topaz $Al_2[SiO_4]F_2$, using high-precision X-ray diffraction data. The electron deformation density, positive values of the Laplacian at (3,−1) bond critical points and the net atomic charges indicate a closed-shell-type interaction in the polyhedra. Anion valence-shell charge depletions are revealed. Maxima in the Laplacian of the electron density are displaced towards the close-packed plane owing to the mutual repulsion of the anion valence shells. The relationship between the topological features of the electron density and the close-packing concept is discussed. Shifts of the critical points from the internuclear vectors reflect the strain in the structure.

1. Introduction

The bonding in silicates has been discussed for many years (Liebau, 1985; Tsirelson *et al.*, 1990; Gibbs *et al.*, 1994). Studies of the electron density (ED) in these compounds allow a greater understanding of the nature of chemical bonds in different structural fragments, *e.g.* silicon tetrahedra and other coordination polyhedra. This paper describes the study of the ED in topaz. It was undertaken within the framework of an investigation of the ED in silicates. Previously, we have studied phenakite (Tsirelson *et al.*, 1986), beryl (Evdokimova *et al.*, 1988), cordierite (Belokoneva, Evdokimova *et al.*, 1992), dioptase (Belokoneva, Smirnitskaya *et al.*, 1992) and tourmaline (Belokoneva & Tsirelson, 1993).

The crystal structure of topaz was determined independently by Pauling (1928) and Alston & West (1929), refined by Ladell (1965) and described later in more detail by Ribbe & Gibbs (1971) and others. Topaz belongs to the nesosilicates according to the common silicate classification. It is characterized by the close-packed layer sequence *ABAC*...; the layers are perpendicular to the *b* axis and an oxygen-anion layer alternates with a fluorine–oxygen-anion layer. There are 12 tetrahedral and six octahedral holes per six anions (four O and two F atoms) in the close-packed layers. An Si atom occupies one of the 12 tetrahedral holes and Al atoms occupy two of the six octahedral holes. Thus, each O atom is coordinated by one Si and two Al, and the F atom by two Al atoms. A crankshaft-like chain of edge-sharing Al octahedra and corner-sharing Si tetrahedra is parallel to the *c* axis (Fig. 1).

Natural derivatives are known with partial isomorphic substitution of F^- ions by OH^- groups. The F^-/OH^- ratio in one anion position may vary depending on the mineral genesis. It is known (Rosenberg, 1967) that the degree of fluorine enrichment is correlated with the unit-cell parameter *b*. The location of H atoms was studied by Parise *et al.* (1980) and Northrup *et al.* (1994).

The previous study of the ED in natural topaz was performed using an accurate X-ray diffraction data set by Belokoneva *et al.* (1993). A spherical-atom model was refined with high-angle data and dynamic Fourier-deformation ED maps were calculated. The present paper describes a multipole model refinement of the ED using the same data. The static multipole-deformation ED maps and topological analysis of the model ED are presented.

We have also paid attention to the close-packing of topaz. Close-packed crystal structures are rare for silicates. A geometrical description for the group of hexagonal close-packed silicates (olivine, humite, clinohumite *etc.*) has been given by Belov (1947).

2. Experimental

A sample of transparent pale-blue topaz was ground into a 0.25 mm diameter sphere. The crystal quality proved to be satisfactory according to the Laue X-ray diffraction patterns. Intensities of 4902 reflections with $I \geq 1.96\sigma(I)$ were obtained using monochromated Mo $K\alpha$ radiation on a four-circle Syntex $P\bar{1}$ diffractometer. Nonstandard crystal axes corresponding to *Pbnm* were used (standard space group $D_{2h}^{16} = Pnma$). The reflection profiles were step-scanned in the $\theta/2\theta$ mode; the scan speed varied from 2 to 24° min^{-1}. One standard reflection (120) was measured every 100

ISSN 0108-7681

reflections; its intensity variation did not exceed 1.5%. The reflections were measured up to $(\sin\theta/\lambda)_{max}$ = 1.08 Å^{-1} in four octants of the reciprocal space corresponding to the following Miller indices: *hkl*, $h\bar{k}\bar{l}$, $\bar{h}k\bar{l}$, $\bar{h}\bar{k}l$ (*i.e.* four equivalent reflections measured for a general-type reflection).

Systematic extinctions confirmed the space group *Pbnm*. Averaging of the intensities of symmetry-equivalent reflections corrected for Lorentz and polarization factors yielded $R_{int} = \sum_i(I_i - \langle I\rangle)/\sum_i\langle I\rangle_i$. The final data set contains 1356 independent reflections. The insignificantly small absorption of radiation in the sample (μr = 0.15) was ignored.

The unit-cell parameter b = 8.802 Å in the sample corresponds to a weak isomorphism with the ratio F^-/OH^- = 0.95:0.05 (Rosenberg, 1967). The spherical-atom model refinement of this ratio gives $F^-/OH^- \simeq$ 0.98:0.02 (2). Thus, the OH^- impurity of topaz was ignored.

Crystallographic data and experimental information are summarized in Table 1.

3. Refinement

The ED was approximated by the Hansen & Coppens (1978) multipole model, in which the atomic ED is expressed by

$$\rho_{at}(\mathbf{r}) = P_c\rho_{core}(r) + P_v\kappa'^3\rho_{va}(\kappa' r) + \sum_{l=1}^{4}\kappa'^3 R_l(\kappa'' r)\sum_{m=-l}^{l}P_{lm}y_{lm}(\mathbf{r}/r), \quad (1)$$

where ρ_{at} represents atom density and ρ_{va} valence density. Refinements were carried out using the program *MOLDOS*96 (Protas, 1996), based on the program *MOLLY* (Hansen & Coppens, 1978) modified for DOS personal computers. The optimized parameters were a scale factor, the valence-shell contraction–expansion parameters κ' and κ'', and the multipole populations P_v and P_{lm} up to hexadecapole level (l_{max} = 4). Isotropic extinction according to Becker & Coppens (1974) was assumed to be mosaic spread dominated (extinction type I) with a Lorentzian distribution of the mosaic block orientation. The exponential-type radial functions $r^{n_l}\exp(-\kappa''\xi r)$ with n_l = 2, 2, 2, 3, 4 (oxygen, fluorine) and n_l = 4, 4, 4, 4, 4 (aluminium, silicon) (Hansen & Coppens, 1978) were used. Initial values of the orbital exponents were selected according to Hehre *et al.* (1969). Anomalous-dispersion corrections were taken from *International Tables for Crystallography* (Wilson, 1995). One set of κ' and κ'' parameters was used for all O atoms. The local coordinate systems are given as supplementary material.†

† Supplementary data for this paper are available from the IUCr electronic archives (Reference: SH0101). Services for accessing these data are described at the back of the journal.

Table 1. *Experimental details*

Crystal data	
Chemical formula	$Al_2(SiO_4)F_2$
Chemical formula weight	184.04
Cell setting	Orthorhombic
Space group	*Pbnm*
a (Å)	4.6511 (8)
b (Å)	8.802 (1)
c (Å)	8.402 (1)
V (Å^3)	343.97 (8)
Z	4
D_x (Mg m^{-3})	3.558
Radiation type	Mo $K\alpha$
Wavelength (Å)	0.71069
No. of reflections for cell parameters	15
θ range (°)	7–14
μ (mm^{-1})	1.181
Temperature (K)	293
Crystal form	Sphere
Crystal radius (mm)	0.0125
Crystal colour	Pale blue, transparent
Data collection	
Diffractometer	Syntex $P\bar{1}$
Data collection method	$\theta/2\theta$ scans
Absorption correction	None
No. of measured reflections	4902
No. of independent reflections	1815
No. of observed reflections	1356
Criterion for observed reflections	$I(hkl) \geq 1.96\sigma\lvert I(hkl)\rvert$ and $\lvert F_o - F\rvert/F > 0.5$ (during refinements)
R_{int}	0.0227
θ_{max} (°)	50
Range of h, k, l	$0 \rightarrow h \rightarrow 9$ $0 \rightarrow k \rightarrow 18$ $0 \rightarrow l \rightarrow 17$
No. of standard reflections	1
Frequency of standard reflections	Every 120 min
Intensity decay	None
Refinement	
Refinement on	$F(hkl)$
R	0.0091
wR	0.011
S	1.13
No. of reflections used in refinement	1352
No. of parameters used	175
Weighting scheme	$w = [\sigma^2(F_o) + (0.006F_o)^2]^{-1}$
$(\Delta/\sigma)_{max}$	< 0.02
$\Delta\rho_{max}$ (e Å^{-3})	+0.15
$\Delta\rho_{min}$ (e Å^{-3})	−0.15
Extinction method	Becker & Coppens (1974)
Extinction coefficient	2.24 seconds (mosaic spread; type I)
Source of atomic scattering factors	Hehre *et al.* (1969)

Starting atomic positional and displacement parameters were taken from Belokoneva *et al.* (1993). High-angle refinements ($\sin\theta/\lambda > 0.7$ Å^{-1}) of atomic positional and anisotropic displacement parameters using free-atom scattering factors yielded $R(F)$ = 0.010, $wR(F)$ = 0.012 and S = 1.04. The corresponding refinements with all data, including only an extinction parameter and a scale factor, yielded $R(F)$ = 0.013, $wR(F)$ = 0.022 and S

Table 2. *Positional and anisotropic displacement parameters obtained from the multipole model*

$U_{eq} = (1/3)\Sigma_i\Sigma_j U^{ij} a^i a^j \mathbf{a}_i.\mathbf{a}_j$.

	x	*y*	*z*
Al	−0.09674 (2)	0.13099 (1)	0.08265 (1)
Si	−0.39751 (2)	0.05960 (1)	0.75
O1	−0.29621 (7)	0.03196 (3)	0.25
O2	0.04272 (7)	0.25606 (4)	0.25
O3	0.21047 (4)	−0.01074 (2)	0.09236 (3)
F	−0.40193 (5)	0.25256 (3)	0.05684 (3)

	U^{11}	U^{22}	U^{33}	U^{12}	U^{13}	U^{23}
Al	0.00348 (3)	0.00315 (3)	0.00317 (3)	0.00007 (2)	−0.00008 (2)	0.00001 (2)
Si	0.00256 (4)	0.00257 (4)	0.00277 (4)	0.00009 (3)	—	—
O1	0.00331 (8)	0.00472 (8)	0.00391 (8)	−0.00130 (7)	—	—
O2	0.00536 (9)	0.00281 (8)	0.00385 (8)	−0.00080 (7)	—	—
O3	0.00413 (6)	0.00409 (6)	0.00357 (6)	0.00078 (5)	−0.00119 (5)	−0.00028 (5)
F	0.00559 (6)	0.00616 (7)	0.00602 (6)	0.00239 (6)	−0.00057 (5)	0.00112 (5)

= 2.03. The multipole refinement procedure was then applied as follows. The scale factor, extinction coefficient and ED parameters (κ', P_v, P_{lm}) for all atoms were first refined with the weighting scheme $w = 1/\sigma^2(F_o)$ using all reflections. The procedure was then repeated by refining the κ'' parameters. Four reflections with $|F_o - F_c|/F_c > 0.5$ were rejected. The refinement was performed again, the weighting scheme $w = 1/[\sigma^2(F_o) + (0.006F_o)^2]$ providing the correct model fit, according to Abrahams & Keve (1971) and to the statistical *F* tests (Draper & Smith, 1981). Final values of the $\kappa''\xi$ parameters were 2.05 (7) for Al, 1.93 (6) for Si, 2.69 (13) for O and 3.24 (20) for F. The coordinates and anisotropic displacement parameters were then reintroduced and refined with the multipole parameters, except κ' and κ'' (167 parameters over a total of 175 refined parameters). The resulting atomic coordinates and anisotropic displacement parameters were found to be practically the same as those obtained from the high-angle refinement.

Final refinement indices were $R(F) = 0.0091$, $wR(F) = 0.0116$ and $S = 1.13$.† The maximal extinction effect ($y_{min} = 0.341$) was for the 006 reflection (the observed intensity $I_{obs} = y_{min} I_{kin}$, where I_{kin} is the kinematical value). Five other reflections have a value of y_{min} less than 0.5. We have calculated the corresponding ED maps with and without their contribution and found that their importance was negligible for the valence ED deformation maps.

Figures of merit are given in Table 1. Table 2 lists the positional and anisotropic displacement parameters. Selected interatomic distances and valence angles are presented in Table 3.

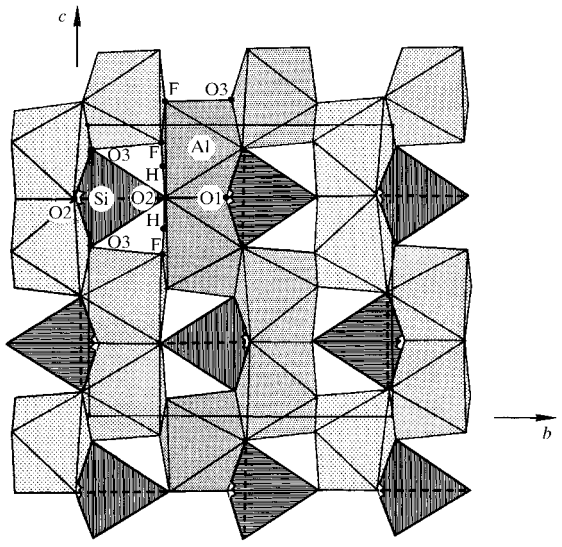

Fig. 1. The *bc* projection of the topaz crystal structure. The close-packed layers are perpendicular to the *b* axis. Si tetrahedra are dashed; Al octahedra on different levels with respect to the *a* axis are dotted.

4. Electron density and topological analysis

4.1. *Multipole model density*

The static electron deformation density $\Delta\rho$, characterizing the redistribution of electrons when spherical atoms form crystals, was calculated using the multipole parameters. The program *SALLY* (Hansen, 1990) was used. The $\Delta\rho$ maps for three different sections of the Si tetrahedron are shown in Fig. 2. The peak heights on Si—O bonds are 0.5–0.6 e Å^{-3} (Figs. 2*a* and 2*b*) and the maxima are, as one would expect, displaced towards the more electronegative oxygen anions. In topaz each oxygen has three neighboring cations: one Si with tetrahedral coordination and two edge-sharing octahedrally coordinated Al; an example of the deformation density around the O2 atom is shown in Fig. 2(*c*).

† See deposition footnote on p. 775.

Table 3. *Main interatomic distances (Å) and valence angles (°)*

Central atom coordinates from Table 2.

Si tetrahedron			
Si—O1^{i}	1.637 (3)	Si—O3^{iii}	1.642 (2)
Si—O2^{ii}	1.647 (3)	Si—O3^{iv}	1.642 (2)
		Mean	1.642
O1^{i}—Si—O2^{ii}	109.78 (11)	O1^{i}—Si—O3^{iv}	109.41 (11)
O1^{i}—Si—O3^{iii}	109.41 (11)	O2^{ii}—Si—O3^{iii}	110.34 (11)
		O2^{ii}—Si—O3^{iv}	110.34 (11)
		O3^{iii}—Si—O3^{iv}	107.54 (10)
		Mean	109.47
Al octahedron			
Al—O1	1.897 (2)	Al—O3^{v}	1.887 (2)
Al—O2	1.900 (2)	Al—F	1.791 (2)
Al—O3	1.898 (2)	Al—F^{vi}	1.801 (2)
		Mean	1.862
O1—Al—O2	83.38 (9)	O2—Al—F^{vi}	88.86 (9)
O1—Al—O3	91.96 (9)	O3—Al—O3^{v}	82.86 (8)
O1—Al—O3^{v}	100.53 (9)	O3—Al—F^{vi}	91.34 (9)
O1—Al—F	88.67 (9)	O3^{v}—Al—F	91.07 (9)
O2—Al—O3	95.27 (9)	O3^{v}—Al—F^{vi}	87.32 (8)
O2—Al—F	90.82 (9)	F—Al—F^{vi}	88.85 (9)
		Mean	90.08

Symmetry codes: (i) $-1-x, -y, \frac{1}{2}+z$; (ii) $x-\frac{1}{2}, \frac{1}{2}-y, \frac{1}{2}+z$; (iii) $-x, -y, \frac{1}{2}+z$; (iv) $-x, -y, 1-z$; (v) $-x, -y, -z$; (vi) $\frac{1}{2}+x, \frac{1}{2}-y, -z$.

Fig. 3 displays the deformation density in an equatorial section of the Al octahedron. This map exhibits peaks of 0.4–0.6 e Å^{-3} on the Al—O bonds. This density is more strongly polarized towards the ligand than for the Si—O bonds. Around O1 and O2, one observes peaks in the direction of both the two Al atoms related by a crystallographic mirror plane through O1–O2.

A so-called 'kappa refinement' (Coppens *et al.*, 1979) was performed as well. Only the scale factor, extinction parameter, P_v and κ' values were refined. This procedure avoids taking into account electrons attributed to certain highly diffuse multipole functions and leads, in general, to charges in better agreement with common chemical notions. The resulting charges and κ' values of the atoms are: Al +1.53 (12), κ' = 1.04 (4); Si +1.75 (10), κ' = 1.05 (2); O1 −0.76 (6), O2 −1.11 (5), O3 −1.03 (5), κ' = 0.976 (3); F −0.44 (5), κ' = 0.977 (3). These charges are close to the values discussed by Tsirelson *et al.* (1990) for several neso, ring and chain silicates. They are also close to the Al and Si charges obtained under the same conditions as Ghermani *et al.* (1996) in the study of natrolite, although both Al and Si are in tetrahedral coordination in this material. Note that the net charge of the O1 atom is slightly smaller than those of the other two O atoms. The cation κ' parameters are slightly larger than those obtained from the multipole refinement.†

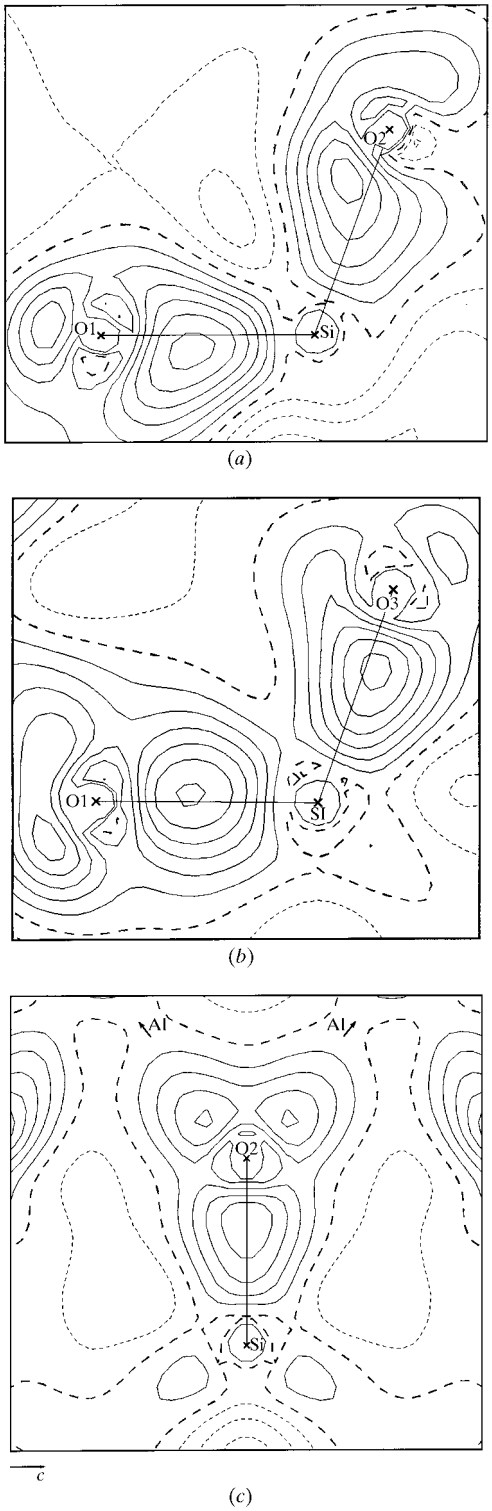

Fig. 2. Static multipole deformation ED in the Si tetrahedron. (*a*) O1—Si—O2 section (mirror plane). Here and on the other ED maps the contour spacing is 0.1 e Å^{-3}, positive contours are solid, negative contours are short-dashed, and zero contours are bold-dashed. (*b*) O1—Si—O3 section. (*c*) Si—O2 section perpendicular to the mirror plane.

† See deposition footnote on p. 775.

Table 4. *Values of the electron density, ρ, and Laplacian of the electron density, $\nabla^2\rho$, at (3,−1) critical points in the polyhedra*

Bond path	$\rho(\mathbf{r}_{cp})$ (e Å^{-3})	$\nabla^2\rho(\mathbf{r}_{cp})$ (e Å^{-5})	x	y	z	CP deviation from the interatomic vector (Å)
Si—O1[i]	1.36 (3)	10.9 (6)	−0.5190	0.0170	0.75	0.05
Si—O2[ii]	1.18 (3)	11.5 (6)	−0.4237	0.1365	0.75	0.01
Si—O3[iii]	1.30 (3)	8.2 (8)	−0.3138	0.0430	0.6860	0.04
Si—O3[iv]	1.30 (3)	8.2 (8)	−0.3138	0.0430	0.8140	0.04
Al—O1	0.65 (3)	4.8 (7)	−0.1962	0.0975	0.1498	0.10
Al—O2	0.61 (1)	5.1 (1)	−0.0322	0.1824	0.1517	0.03
Al—O3	0.60 (2)	3.9 (4)	0.0204	0.0654	0.0906	0.08
Al—O3[v]	0.71 (1)	5.3 (1)	−0.1613	0.0846	0.0115	0.09
Al—F	0.72 (1)	9.0 (3)	−0.2224	0.1853	0.0666	0.05
Al—F[vi]	0.75 (1)	6.8 (1)	−0.0057	0.1763	0.0238	0.05

Symmetry codes: (i) $-x-1, -y, z+1/2$; (ii) $x-1/2, -y+1/2, z+1/2$; (iii) $-x, -y, z+1/2$; (iv) $-x, -y, -z+1$; (v) $-x, -y, -z$; (vi) $x+1/2, -y+1/2, -z$.

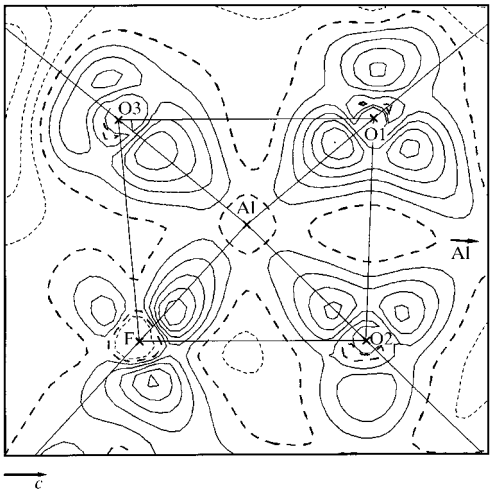

Fig. 3. The 'patchwork' map of the static multipole deformation ED in the Al octahedron. Equatorial O3—O1—O2—F section.

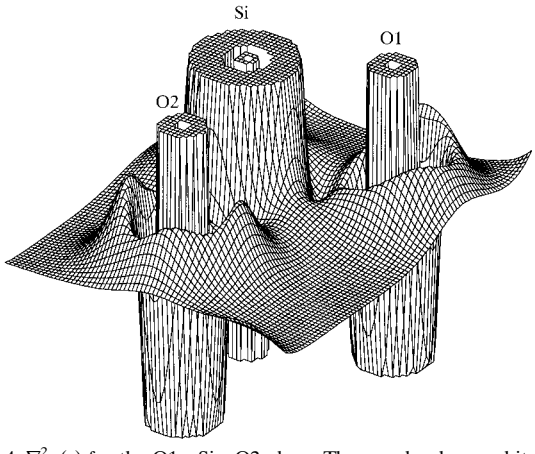

Fig. 4. $\nabla^2\rho(\mathbf{r})$ for the O1—Si—O2 plane. The map has been arbitrarily truncated at ±30 e Å^{-5}. Values above the horizontal plane show regions where $\rho(\mathbf{r})$ is locally depleted and *vice versa*.

4.2. *Topology of the total electron density*

The ED distribution may also be described in terms of the ED critical points (CP's), where the gradient $\nabla\rho(\mathbf{r})$ of the ED vanishes (Bader, 1990; Tsirelson & Ozerov, 1996). The saddle CP's (3,−1) on the interatomic lines are termed bond CP's. The Laplacian of ρ is often used to emphasize the fine details of the ED. If $\nabla^2\rho(\mathbf{r}) < 0$, then $\rho(\mathbf{r})$ is locally concentrated; if $\nabla^2\rho(\mathbf{r}) > 0$, then $\rho(\mathbf{r})$ is locally depleted. The program *LSPROP* by Howard & Mallinson (1993) was used. A list of critical points is given in Table 4.

(3,−1) critical points were found in all bonds and the Laplacian in these points is always positive. This is in agreement with predominantly closed-shell-type interactions. The shifts of the CP's from the internuclear vectors reflect the strain in the topaz structure and characterize the distortion of the polyhedra. One indeed observes that these shifts are smaller for the Si—O bonds than for the Al—O bonds, in agreement with the more regular Si coordination geometry (see Table 3).

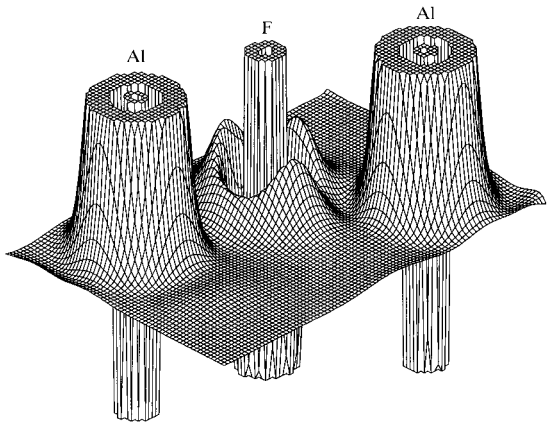

Fig. 5. $\nabla^2\rho(\mathbf{r})$ for the Al—F—Al plane. The map has been arbitrarily truncated at ±80 e Å^{-5}.

The three-dimensional maps of $\nabla^2\rho(\mathbf{r})$ in O1—Si—O2 and Al—F—Al planes are given in Figs. 4 and 5, respectively.

For bonded atoms the outer quantum shell symmetry is violated and some local maxima, minima and saddle points appear in the Laplacian. The three-dimensional maps of the Laplacian (Figs. 4 and 5) exhibit spikes from *K* shells located at the centers of the Si and of the Al atom, and large peaks from the *L* shells. The diffuse valence *M* shells of free Si and Al atoms are missing. The interesting features are associated with O and F atoms, which show a hill structure of the valence-electron shells. The hills around anions correspond to a valence-shell charge depletion (VSCD) with maxima located between internuclear lines. The saddle points appear on these lines between VSCD maxima. This is similar to that found by Downs & Swope (1992) for the borosilicate danburite, $CaB_2Si_2O_8$.

There are two types of close-packed layers in topaz. The first layer is composed of O1 and O3 atoms and is of cubic close-packed type (Fig. 6*a*). The second is formed by F and O2 atoms, with a predominance of F atoms (Fig. 6*b*), and is of hexagonal close-packed type. Owing to a significantly distorted O1—O3 layer (the axial spread of atoms along *b* is 0.37 Å), a planar map centered at O1 was composed of six patches in order to examine the deformation ED in more detail. The O2—F

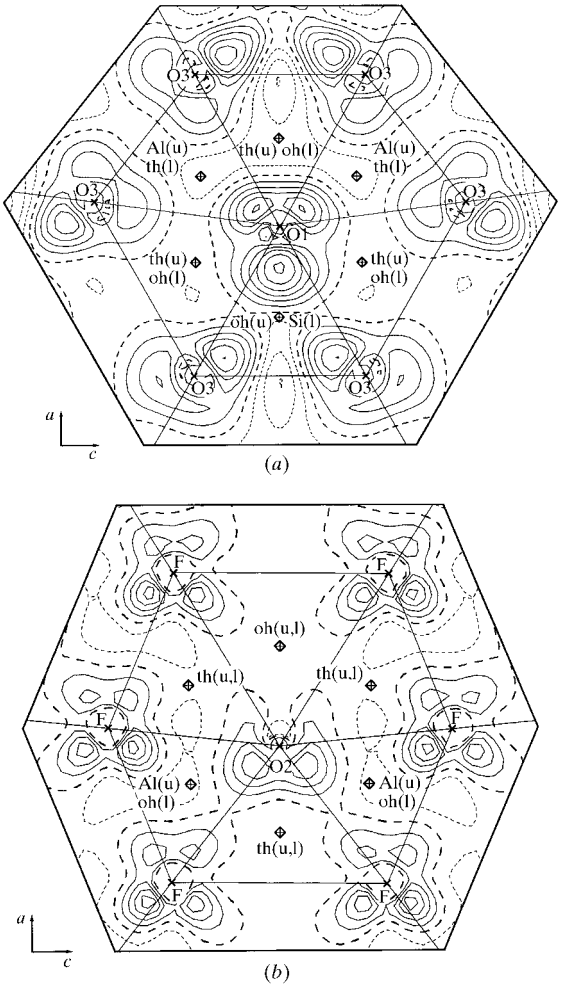

Fig. 6. Static multipole deformation ED in close-packed layers of anions. (*a*) The 'patchwork' map of the cubic O1—O3 layer. Each patch is a triangular map through one of the six O3—O1—O3 fragments. Projection of the Al and Si atom positions occupying the holes above (u) or below (l) the layer, and the unoccupied octahedral (oh) and tetrahedral (th) holes are indicated by crossed diamonds. (*b*) The 'patchwork' map of the hexagonal O2—F layer.

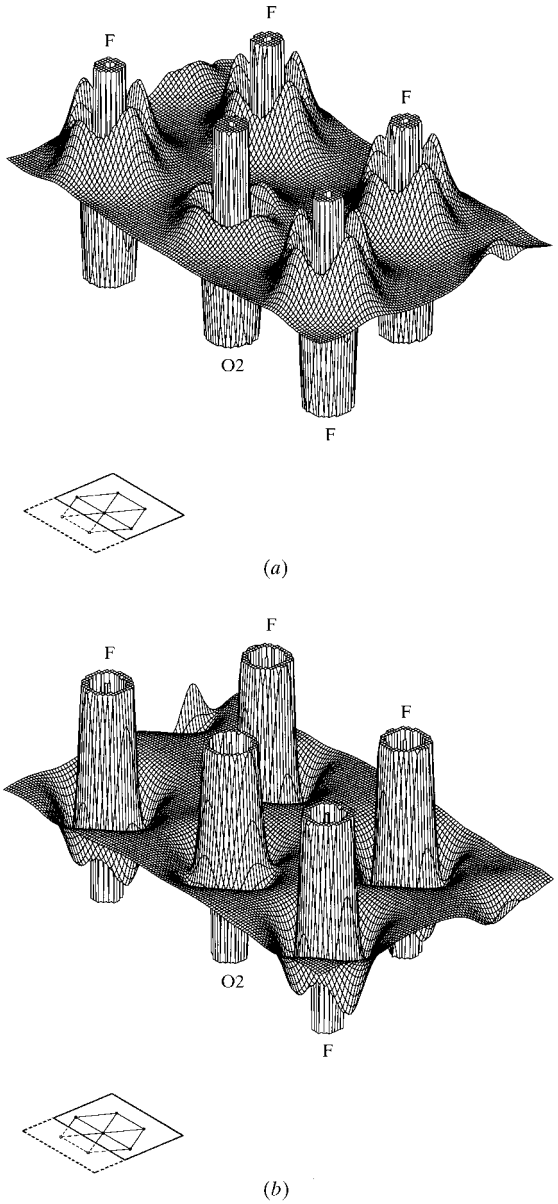

Fig. 7. $\pm\nabla^2\rho(\mathbf{r})$ for a close-packed hexagonal O2—F fragment. The maps have been arbitrarily truncated at ± 50 e Å^{-5}. (*a*) $+\nabla^2\rho(\mathbf{r})$; (*b*) $-\nabla^2\rho(\mathbf{r})$.

close-packed layer is less distorted than the O1—O3 layer (the spread of atoms along b is 0.07 Å). A 'patchwork' map was also constructed for this layer (Fig. 6*b*). The peak heights near the same atoms in different parts of the 'patchwork' maps depend on the orientation of the local patch section.

Fig. 7 displays $+\nabla^2\rho(\mathbf{r})$ and $-\nabla^2\rho(\mathbf{r})$ three-dimensional maps for a fragment of O2—F close-packed hexagon. The 'patchwork' maps of an $\nabla^2\rho(\mathbf{r})$ for two topaz close-packed layers are given in Fig. 8. There are no chemical bonds in these sections, but a strong asphericity of the atomic ED is observed. The main reason for the O1—O3 layer distortion is the different influence of the Si and Al cations. In Fig. 8(*a*), a broad saddle and a weak $\nabla^2\rho$ minimum on the Si—O lines are observed, whereas the Al—O lines exhibit only saddle points. The Al cations, apparently, are responsible for the distortion of the O2—F layer (Fig. 8*b*).

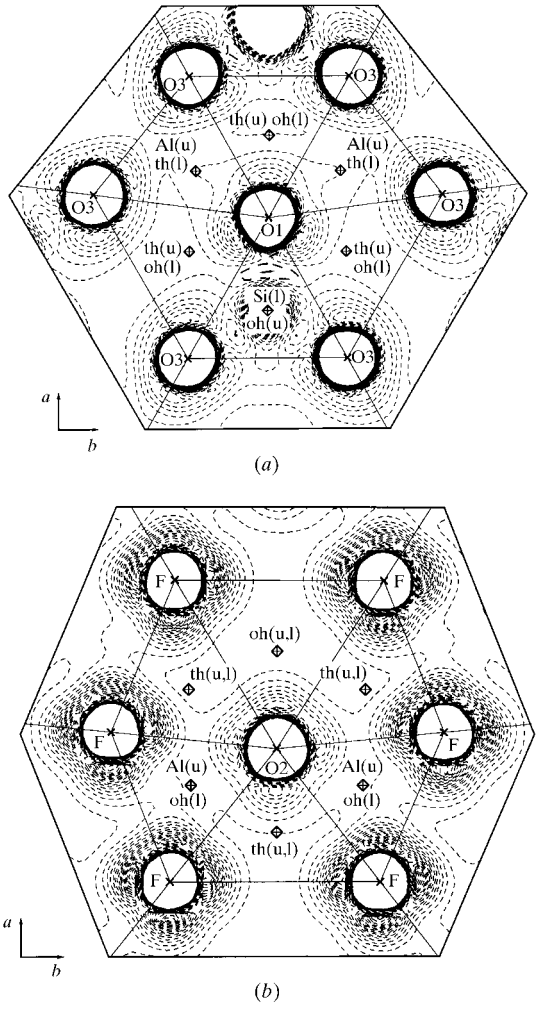

Fig. 8. The 'patchwork' maps of $\nabla^2\rho(\mathbf{r})$ of the close-packed layers in topaz. Contour spacing is 2.0 e Å^{-5}. Positive contours are short-dashed, negative contours are solid and zero contours are bold-dashed. The traces from inner shells have been erased. (*a*) $\nabla^2\rho(\mathbf{r})$ of the cubic O1—O3 layer; (*b*) $\nabla^2\rho(\mathbf{r})$ of the hexagonal O2—F layer.

There are four VSCD maxima around each of the anions in the O1—O3 close-packed-type layer (three of them can be seen in Fig. 8*a*) and five maxima in the O2—F hexagonal close-packed-type layer (four of them are seen in Fig. 8*b*). These maxima are mainly displaced towards the close-packed plane owing to the mutual repulsion of the anion valence shells. The correspondence of the locations of the VSCD maxima around each anion and the local symmetry in the close-packed layer is not observed. The anticorrelation between deformation ED peaks (Fig. 6) and VSCD maxima (Fig. 8) can be noted.

The anions of close-packed layers of topaz form tetrahedral and octahedral holes; anion valence shells are deformed depending on the presence or absence of cations in the holes of different type and on the nature of these cations. The pictures of $\nabla^2\rho(\mathbf{r})$ reveal the details of this deformation (see Figs. 8*a* and 8*b*). It is instructive to compare the picture of the Laplacian in the oxygen layer of topaz with the same picture of the close-packed oxygen layer in MgO (Fig. 9). The latter has been calculated from the experimental data of Tsirelson *et al.* (1998). The Mg atoms in MgO occupy all the octahedral holes, while all the tetrahedral holes are empty. The symmetrical positions of cations of the same nature in the equivalent octahedral holes in MgO provide the balance of the atomic interactions in the close-packed layers. It does not perturb the local ED distribution in the oxygen layer plane. On the contrary, in topaz the strong deformation of the oxygen valence shells is observed. Apparently, the analysis of $\nabla^2\rho(\mathbf{r})$ could be used for a quantitative estimation of crystal structure distortion.

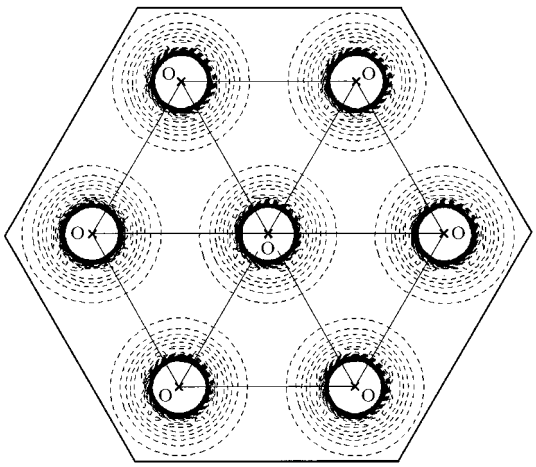

Fig. 9. The $\nabla^2\rho(\mathbf{r})$ distribution in the cubic oxygen close-packed layer in MgO.

References

Abrahams, S. C. & Keve, E. T. (1971). *Acta Cryst.* A**27**, 157–165.

Alston, N. A. & West, J. (1929). *Z. Kristallogr.* **69**, 149–167.

Bader, R. F. W. (1990). *Atoms in Molecules: a Quantum Theory*. Oxford University Press.

Becker, P. J. & Coppens, P. (1974). *Acta Cryst.* A**30**, 129–147.

Belokoneva, E. L., Evdokimova, O. A., Tsirelson, V. G. & Urusov, V. S. (1992). *Vestn. Mosk. Gos. Univ. Ser. Geol.* **1**, 60–71. (In Russian.)

Belokoneva, E. L., Smirnitskaya, Yu. Ya. & Tsirelson, V. G. (1992). *Zh. Neorg. Khim.* **37**, 1588–1596. (In Russian.)

Belokoneva, E. L., Smirnitskaya, Yu. Ya. & Tsirelson, V. G. (1993). *Russ. J. Inorg. Chem.* **38**, 1252–1256.

Belokoneva, E. L. & Tsirelson, V. G. (1993). *Russ. J. Inorg. Chem.* **38**, 1257–1264.

Belov, N. V. (1947). *Structure of Ionic Crystals and Metallic Phases*. Moscow: Academy of Science USSR. (In Russian.)

Coppens, P., Guru Row, T. N., Leung, P., Stevens, E. D., Becker, P. J. & Yang, Y. W. (1979). *Acta Cryst.* A**35**, 63–72.

Downs, J. W. & Swope, R. J. (1992). *J. Phys. Chem.* **96**, 4834–4840.

Draper, N. R. & Smith, H. (1981). *Applied Regression Analysis*, 2nd ed. New York: Wiley.

Evdokimova, O. A., Belokoneva, E. L., Tsirelson, V. G. & Urusov, V. S. (1988). *Geokhimiya*, **5**, 677–687. (In Russian.)

Ghermani, E.-N., Lecomte, C. & Dusausoy, Y. (1996). *Phys. Rev. B*, **53**, 5231–5239.

Gibbs, G. V., Downs, J. W. & Boisen, M. B. (1994). *Rev. Mineral.* **29**, 331–368.

Hansen, N. K. (1990). *SALLY. Program for Calculating Static Deformation or Valence Densities*. MS DOS version. Unpublished. LCM3B, Faculté des Sciences, Université Henri Poincaré, Nancy 1, France.

Hansen, N. K. & Coppens, P. (1978). *Acta Cryst.* A**34**, 909–921.

Hehre, W. J., Stewart, R. F. & Pople, J. A. (1969). *J. Chem. Phys.* **51**, 2657–2664.

Howard, S. & Mallinson, P. (1993). *LSPROP*93. *A Program for Topological Analysis of Charge Density*. Unpublished. Chemistry Department, University of Glasgow, Scotland.

Ladell, J. (1965). *Norelco Rep.* **12**, 34–39.

Liebau, F. (1985). *Structural Chemistry of Silicates*. Berlin, Heidelberg, New York: Springer Verlag.

Northrup, P. A., Leinenweber, K. & Parise, J. B. (1994). *Am. Mineral.* **79**, 401–404.

Parise, J. B., Cuff, C. & Moore, F. H. (1980). *Mineral. Mag.* **43**, 943–944.

Pauling, L. (1928). *Proc. Natl Acad. Sci. USA*, **14**, 603–606.

Protas, J. (1996). *MOLDOS*96/*MOLLY*. MS DOS updated version. Unpublished. LCM3B, Faculté des Sciences, Université Henri Poincaré, Nancy 1, France.

Ribbe, P. H. & Gibbs, G. V. (1971). *Am. Mineral.* **56**, 24–30.

Rosenberg, P. E. (1967). *Am. Mineral.* **52**, 1890–1895.

Tsirelson, V. G., Avilov, A. S., Abramov, Yu. A., Belokoneva, E. L., Kitaneh, R. & Feil, D. (1998). *Acta Cryst.* B**54**, 8–17.

Tsirelson, V. G., Evdokimova, O. A., Belokoneva, E. L. & Urusov, V. S. (1990). *Phys. Chem. Miner.* **17**, 275–292.

Tsirelson, V. G. & Ozerov, R. P. (1996). *Electron Density and Bonding in Crystals*. Bristol, Philadelphia: IOP.

Tsirelson, V. G., Sokolova, E. V. & Urusov, V. S. (1986). *Geokhimiya*, **8**, 1170–1180. (In Russian.)

Wilson, A. J. C. (1995). Editor. *International Tables for Crystallography*, Vol. C. Dordrecht: Kluwer Academic Publishers.